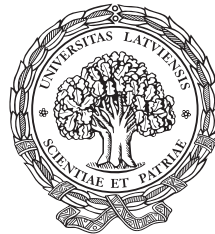


UNIVERSITY OF LATVIA



LATVIJAS
UNIVERSITĀTE

ANNO 1919



Edgars Elsts

Summary of the Doctoral Thesis

Spectroscopic Studies of Scintillator Materials: CsI:Tl, CdWO₄:Mo and Tb Activated Oxyfluorides

Doctoral Thesis to Attain a Doctoral Degree in Physics
Subbranch: Solid State Physics

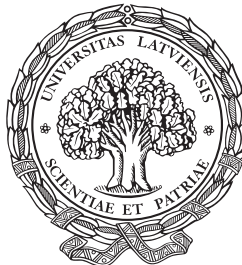
ISBN 978-9984-45-284-5



9 789984 452845 >

Rīga, 2010

UNIVERSITY OF LATVIA
INSTITUTE OF SOLID STATE PHYSICS



Edgars Elsts

**Spectroscopic Studies of Scintillator Materials:
CsI:Tl, CdWO₄:Mo and Tb Activated
Oxyfluorides**

Summary of Doctoral Thesis

Doctoral Thesis to Attain a Doctoral Degree in Physics
Subbranch: Solid State Physics

Scientific advisor: *Dr. habil. phys.*, Professor **Uldis Rogulis**

Rīga, 2010



Type of the PhD thesis: dissertation

Scientific advisor:

Prof., Dr. habil. phys. Uldis Rogulis

Reviewers:

Dr. habil. phys. Linards Skuja

Dr. habil. phys. Juris Purāns

Prof., Dr. habil. phys. Artūrs Medvids

The defense of the PhD thesis will take place in an open session of the Promotion Council of Physics and Astronomy of the University of Latvia on the 6th of January, 2011, at 14:00 in the conference hall of the Institute of Solid State Physics of the University of Latvia.

The PhD thesis and its summary are available at the Library of the University of Latvia (4 Kalpaka Blvd, Riga) and Latvian Academic Library (10 Rupniecibas St, Riga).

Chairperson of the Specialized Promotion Council of the scientific section of Physics and Astronomy at the University of Latvia: *Prof. Emeritus, Dr. habil. phys. Ivars Tāle*

© Edgars Elsts, 2010
© University of Latvia, 2010

ISBN 978-9984-45-284-5

Contents

Abstract	4
1. Introduction	5
1.1. Motivation	5
1.2. Aim of the work	6
1.3. Tasks of the work	6
1.4. Novelty of the work	6
1.5. Author's contribution	6
2. Magnetic resonance spectroscopy	7
2.1. Characteristics and physical nature of the EPR	7
2.2. ODMR	8
2.3. Spin-Hamiltonian	9
3. Experimental methods	11
3.1. Electron paramagnetic resonance	11
3.2. Optically detected magnetic resonance	12
3.3. Software programs for spectra simulation	13
4. Results and discussion	15
4.1. EPR hyperfine structure of the Mo-related defect in CdWO ₄	15
4.2. Tl-related radiation defects in CsI:Tl	20
4.3. Cathodoluminescence of terbium- and ytterbium- activated oxyfluoride glasses and glass ceramics	27
5. Summary	33
5.1. Main results	33
5.2. Thesis	33
5.3. Outlook	33
6. List of author's publications	35
7. List of conference abstracts	36
8. References	37

Abstract

The present work includes studies of three scintillator materials: CdWO₄:Mo, CsI:Tl and oxyfluoride glasses and glass ceramics. The EPR hyperfine structure spectrum of the CdWO₄ crystal with Mo impurities could be explained using a model of a hyperfine interaction with two Cd groups of 2 and 3 equivalent nuclei, respectively. EPR angular dependency spectrum of the irradiated CsI:Tl crystal detected by the magnetic circular dichroism of absorption (MCD) has been studied. Spectra could be explained only by an unpaired spin hyperfine interaction with 3 Tl nuclei. Cathodoluminescence spectra and decay times of Tb and Yb activated oxyfluoride glass and glass ceramics with the composition SiO₂ – Al₂O₃ – Na₂O – LaF₃ – NaF have been studied. Dependences of the decay times and luminescence bands ratios on Tb concentration have been analyzed.

Keywords: CdWO₄:Mo, CsI:Tl, Tb oxyfluoride.

1. Introduction

1.1. Motivation

Solid state scintillators are materials that convert ionising radiation into visible light pulses.

Despite the long history of many traditional scintillator material applications, scientific research to improve the traditional scintillator material properties, as well as development of new scintillator materials still continues. Properties of scintillators are often influenced by the presence of point defects.

Magnetic resonance spectroscopy methods (EPR – Electron Paramagnetic Resonance, ODMR – Optically Detected Magnetic Resonance) are very informative to clarify the structure of these defect centres, however, up to now for studies of scintillator materials these methods have been applied relatively rarely.

At the beginning of this doctoral work magnetic resonances of defect centres of CsI:Tl, CdWO₄:Mo have been observed, but the identification of these defects has not been done or an additional simulations of the spectra were necessary. Single crystal scintillator materials, which were studied in this doctoral work, are widely used: CdWO₄ – as a ionizing radiation detectors and in computed tomography [1], CsI:Tl – in particle physics and experimental physics [2], Fourier transform infrared spectrometers [3].

Optical absorption spectra of CdWO₄ crystal with various impurities, including molybdenum, were studied in [4]. EPR spectrum of CdWO₄:Mo was observed at 20 K [5] and molybdenum impurities in this spectrum were identified unambiguously. However, unpaired spin interactions with the Cd nuclei were not considered sufficiently.

Luminescence of caesium iodide crystal with thallium impurities was well studied [6] but Tl-related defects were not identified by magnetic resonance methods. During the past ten years, a new class of materials – glass and glass ceramics oxyfluoride composites has been developing rapidly, but their applications as a scintillator material were not clear.

Rare earth impurities activated glass and glass ceramics are prospective applications for high-energy physics (particle physics), X-ray computed tomography imaging and industry [7] and up-conversion luminescence [8]. In this work we have studied luminescence mechanisms, which could affect their properties. Glass-ceramic material advantages over the single crystals are their low cost and ability to produce large-size samples [9]. In this work, we have

studied in ISSP prepared terbium activated oxyfluoride scintillator materials, which have characteristic terbium luminescence bands.

1.2. Aim of the work

The aim of the work is to study some of the traditional and new scintillator material properties – a defect structure of the $\text{CdWO}_4:\text{Mo}$ and $\text{CsI}:\text{Tl}$ crystals and luminescence properties of terbium activated glasses and glass ceramics.

1.3. Tasks of the work

1. To determine the hyperfine interaction EPR parameters of the molybdenum defect in CdWO_4 crystal and thallium defect in CsI crystal.
2. To develop the corresponding paramagnetic centres models.
3. To investigate luminescence processes in activated terbium glass and glass ceramics with the composition: $\text{SiO}_2 - \text{Al}_2\text{O}_3 - \text{Na}_2\text{O} - \text{LaF}_3 - \text{NaF}$.

1.4. Novelty of the work

In this work, we have explained Mo-related defect structure of CdWO_4 crystal and Tl-related defect structure of $\text{CsI}:\text{Tl}$ crystal, which were unclear previously.

Cathodoluminescence spectra and decay kinetics of the Tb^{3+} activated oxyflouride glass and glass ceramics have been investigated in this work in order to apply these oxyflourides as scintillator materials.

1.5. Author's contribution

Author has analyzed the experimental data, performed theoretical analysis and EPR spectra modelling using specialized computer software programs.

The predefence of this dissertation was held on May 28, 2010 at the Scientific Seminar of Institute of Solid State Physics University of Latvia.

2. Magnetic resonance spectroscopy

2.1. Characteristics and physical nature of the EPR

Electron paramagnetic resonance (EPR) method was discovered by Yevgeny Zavoisky (*Евгений Завойский*) in 1944 at Kazan University [10–11].

Electron paramagnetic resonance method is one of a most informative method for determining defect structures; however, it has the following limitations:

- Defects should be paramagnetic,
- Static magnetic field and microwave or radio frequency magnetic field must penetrate into the crystal to induce magnetic resonance transitions.

Only crystals or crystallites, which are non-metals and which are not superconductors, can be studied by this method. This method has limited sensitivity and working at the low temperatures yields more information about defects.

Using vector model of the electron behaviour in magnetic field, it is possible to explain the values of electron spin sub-levels and resonant frequency (Figure 2.1). Magnetic dipole precession frequency – Larmor frequency (Figure 2.1 a) in a magnetic field H_0 (γ – gyro magnetic ratio) is:

$$\omega = \gamma H_0$$

The electron spin has two possible magnetic quantum number values (Figure 2.1 b):

$$M_S = +1/2 \text{ un } M_S = -1/2.$$

Formation of energy sublevels for electron with spin $S = 1/2$ occurs according the selection rules for electric magnetic dipole transitions – the transitions must be between the sublevels with $M_S = \pm 1/2$ (Figure 2.1. c):

$$E_2 - E_1 = g\beta H_0,$$

where – g – spectroscopic splitting factor, β – Bohr magneton.

Resonance occurs when the frequency of applied radiation is equal to magnetic dipole precession frequency:

$$h\nu = g\beta H_0, \text{ kur } \omega = 2\pi\nu.$$

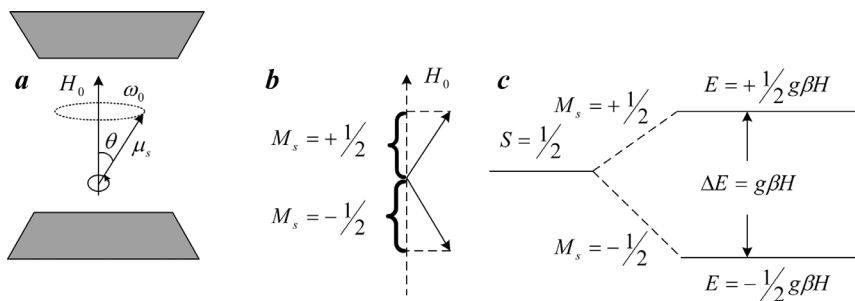


Fig. 2.1 Vector model, which describes the splitting of spin sublevels in magnetic field. [11], page 75.

a – dipole precession in the magnetic field,

b – space quantization of electron's magnetic moment,

c – forming of two spin energy sublevels.

Spectrometer records the derivative of the resonance absorption line. Recording of the individual lines in complex spectra is determined by the necessary precision and the technical possibility to register the first derivative. In some cases, spectrometers can record the second derivative.

Resonant magnetic field value corresponds to crossing of first derivative line with zero line. Numbers of lines in the complex spectra are evaluated by the maximum and minimum number of the derivative.

2.2. ODMR

ODMR (Optically Detected Magnetic Resonance) ODMR is method, where the electron or nuclear spin resonance is observed by changes of the optical transition intensity.

Intensity of phosphorescence with certain wavelength is observed only, if hyperfine interaction frequency corresponds to certain molecule triplet zero field transitions belonging to emission.

Optical EPR detection differs from conventional EPR detection – microwave induced transitions between Zeeman levels are determined indirectly – as the changes of light, which the studied defect emits or absorbs.

In the ODMR measurement, the polarization and intensity of the emitted light depends on the population distribution of spin levels in excited state. To determine the EPR, either polarizations or intensities could be measured.

EPR optical detection is very useful for studies of the ground state of defects either. In this case, optical properties can be directly attributed to certain defects and their structure.

MCD detection of the EPR

MCD (Magnetic Circular Dihroism) is a difference between right and left circularly polarized light absorption, where the light propagates along the direction of the applied magnetic field B_0 .

Circularly polarized light consists of oscillations in two perpendicular planes with the same amplitude but 90° difference in phase [12].

The MCD is a very sensitive method, but its disadvantage is disability to determine number of the defects, unless the strength of the oscillator and the spin-orbital splitting is known, or the MCD is not related to other known processes. The MCD measurements can not be used to determine the defect concentration.

2.3. Spin-Hamiltonian

Energy levels of static system could be described by time-independent Schrödinger wave equation:

$$H\Psi = E\Psi,$$

where Ψ is a wave function, containing information about all essential characteristics of the sample – electron or nuclear structure, H is an operator that describes all the interactions applied to studied system.

H and Ψ defines the so-called eigenvalues problem which solutions are eigenvalues E – stable energy levels of the system.

According to the Born – Oppenheimer's approximation, the kinetic energy of the nuclear motion is not taken into account, and nuclear configuration is considered as “averaged”.

For the calculations of EPR spectrum this concept first was employed by Abragam, Pryce [13].

The solution of this Schrödinger's equation is too complex to use it for an explanation of the EPR spectrum. To simplify this, we can use an effective spin concept, called the Spin-Hamiltonian.

Spin-Hamiltonian allows analysis of the EPR spectra without knowing wave functions of the defect system [12].

$$\hat{H} = \hat{H}_{EZ} + \hat{H}_{FS} + \hat{H}_{HF} + \hat{H}_{NZ} + \hat{H}_Q,$$

where:

$\hat{H}_{EZ} = \mu_B \vec{S} \cdot \tilde{g} \cdot \vec{B}_0$ – Electron Zeeman interaction characterizes the splitting of the energy levels in the external magnetic field,

- μ_B – Bohr magneton,
- \vec{S} – a vector containing the Pauli matrix,
- \tilde{g} – factor (three-dimensional tensor),
- \vec{B} – static magnetic field.

$\hat{H}_{FS} = \vec{S} \cdot \tilde{D} \cdot \vec{S}$ – fine structure of the EPR spectra – Stark effect, which is the splitting of the levels in the presence of an internal electric field,

- \tilde{D} – Three-dimensional fine structure tensor.

$\hat{H}_{HF} = \vec{I} \cdot \tilde{A} \cdot \vec{S}$ – EPR hyperfine interaction, what could be explained by interaction of the electron's magnetic moment with the nuclear spins' magnetic moment,

- \vec{I} – nuclear spin,
- \tilde{A} – hyperfine tensor, three-dimensional.

$\hat{H}_{NZ} = g_n \mu_n \vec{I} \cdot \vec{B}_0$ – Nuclear Zeeman interaction of nuclear spin magnetic moment with the applied magnetic field,

- g_n – factor,
- μ_n – nuclear Bohr magneton.

$\hat{H}_Q = \vec{I} \cdot \tilde{Q} \cdot \vec{I}$ – nuclear quadrupole interaction,

- \tilde{Q} – quadrupole momentum.

The most difficult task for interpretation of EPR spectrum is to understand, how many terms of the Spin-Hamiltonian is necessary to take into account.

In case of EPR, it is important to calculate magnetic field values at a given microwave radiation frequency that corresponds to resonance transitions.

3. Experimental methods

3.1. Electron paramagnetic resonance

EPR Spectra were measured by using of a spectrometer P \varnothing – 1306 (Fig. 3.1). This spectrometer operates at the magnetic field range between 0 and 0.7 Tesla.

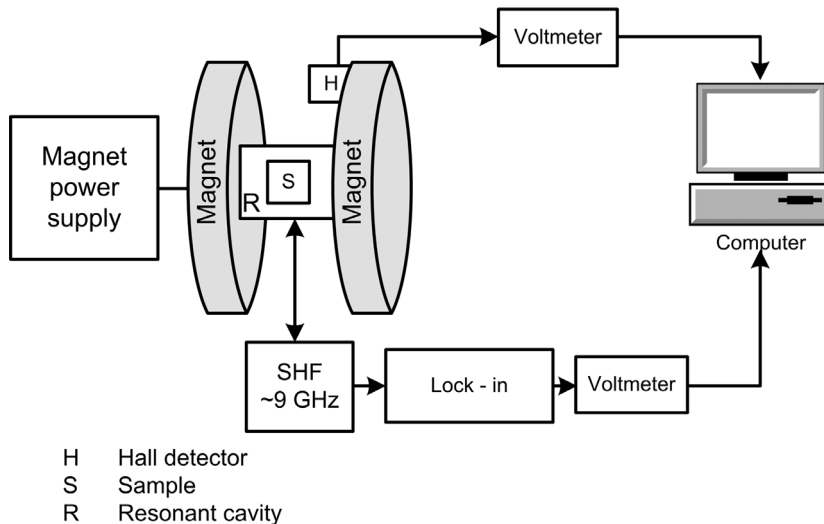


Fig. 3.1. EPR experimental setup: a spectrometer P \varnothing -1306.

Microwave frequency of ~ 9 GHz is generated by the klystron. Microwave radiation is transmitted to the resonant cavity by special rectangular waveguides. Microwave unit ensures an automatic klystron microwave frequency stabilization using the implemented bridge scheme. This allows a considerable improving of the measurement accuracy [14–15].

A sample is placed in a precise – geometric shaped resonant cavity, where microwave radiation from the generator enters and produces standing waves. Vectors B_v (generated by klystron) and B_0 (generated by magnet) are transverse and allow exciting more efficiently the transitions of the electron in atoms. Magnetic field induction is measured by a Hall-effect sensor, attached by the voltmeter. Another voltmeter is used for the EPR signal measurements. Data from both voltmeters are collected by the computer.

3.2. Optically detected magnetic resonance

Experimental spectra of CsI:Tl were measured using experimental ODMR equipment at the University of Paderborn [16]. Figure 3.2 shows a block diagram of this equipment. The light source is a deuterium lamp, which operates in the range 180 nm – 400 nm with a power of 450 W or a halogen lamp, which operates in the range 360 nm – 2000 nm with a power of 150 W.

Light from a light source, reflecting against curved mirror through the slit passes to the dual monochromator. Through a group of lenses light passes to a sample, and further trough the other group of the lenses to the detector.

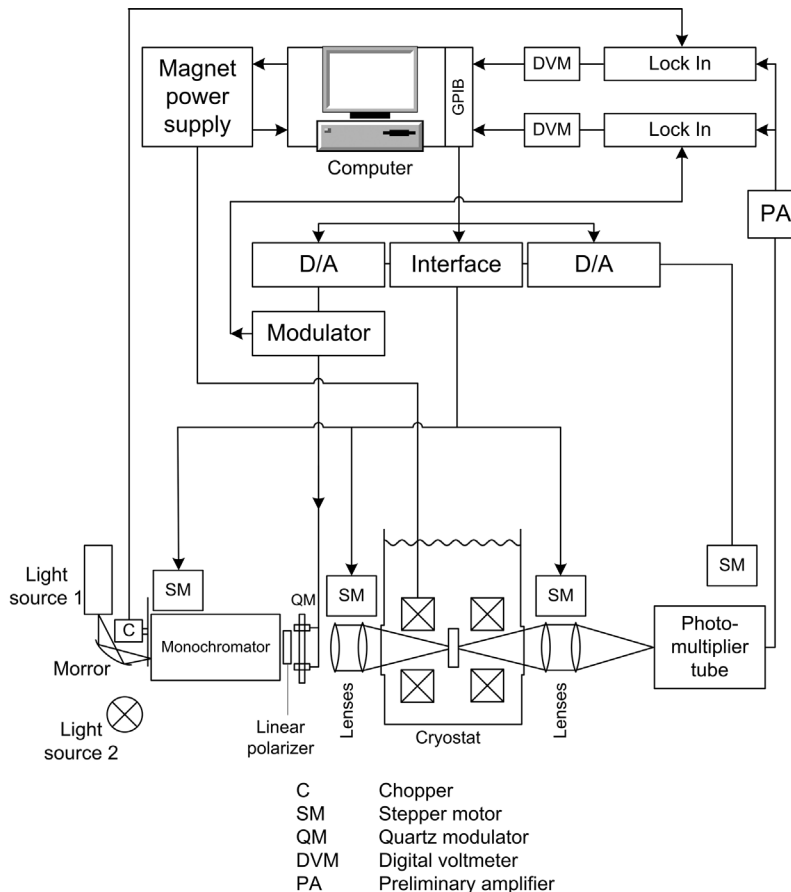


Fig. 3.2. ODMR equipment: a block diagram [16].

The sample is located in a helium cryostat, centred in a cylindrical microwave resonant cavity with an optical input. This cryostat is equipped with a superconducting magnet that can provide a magnetic field up to 4 Teslas. The sample chamber is separated from the helium tank with a needle valve. The temperature in the sample chamber could be lowered till 1.4 K.

A photomultiplier with a range 200 nm – 800 nm is used as a detector, as well as silicon diode with a range 400 nm – 1150 nm, or nitrogen-cooled germanium detector with a range 700 nm – 1700 nm. In the case if a modulator is used, the light is modulated with 27 kHz frequency and demodulated by a lock-in amplifier. ODMR equipment is computer controlled. In addition, a high-energy mobile X-ray source could be used.

3.3. Software programs for spectra simulation

EPR-NMR

Theoretical simulations of the experimental spectra of CsI:Tl were performed using a software program EPR-NMR. This program was developed by Michael J. Mombourquette and John A. Weil at the University of Saskatchewan in Canada [17]. This program allows simulation of EPR spectra of crystals, powders and liquids.

Electron or nuclear spin values must be non-negative half-integers and integers. According to the experience, for the EPR-NMR the maximum number of spin with $S=1/2$ is 11. This program is written in programming language FORTRAN 77. A direct method for these calculations is used. In the case of large systems the calculations can take several days. EPR-FOR sets up the Spin-Hamiltonian matrices and determines their eigenvalues (energies) using an “exact” diagonalization [17].

Since the program is able to calculate angular dependence of magnetic resonance spectrum, it is necessary to define accurately all components and axis directions of interaction tensors, which are entered into Spin-Hamiltonian, Euler angles related to crystal axes and to indicate the plane, in which magnetic field orientation will be changed.

It is also necessary to define, which transitions between which Zeeman sublevels the program must calculate.

The program turned out as the most appropriate for the angular dependence calculations of the CsI:Tl spectrum.

PCS

Computer program PCS was used for the theoretical calculations of the spectrum of CdWO₄. This program was created by Manfred Feege, PhD student of the University of Paderborn (Germany), in 1992. In opposite to the EPR-NMR, PCS can calculate spectra if a large number of nuclear spins interacts with unpaired electron spin, but those interactions must be isotropic.

In the parameters' interface of the program, the following values could be entered: the electron spin, the number of nuclei in equivalent nuclei shells, their spins hyperfine interaction tensor parameters (isotropic and only one anisotropic).

The program could not perform calculations of the angular dependences; it calculates the spectrum at 200 points.

Despite of several limitations, the program turned out to be the most appropriate for EPR spectra calculations of CdWO₄: Mo, since in this task it was necessary to calculate spectra of many equivalent nuclear shells with variable number of equivalent nuclei and different hyperfine interaction constants of them.

4. Results and discussion

4.1. EPR hyperfine structure of the Mo-related defect in CdWO₄

4.1.1. Characteristics of CdWO₄:Mo

CdWO₄ is a well-known crystal scintillator, and its luminescence properties could be affected by structural defects as well as uncontrolled impurities. These structural defects could appear during the crystal growth.

CdWO₄ has a tungsten type structure with a monoclinic singony C_{2h}⁴ and the crystal cleaves along planes (100) [18]. Each cadmium and tungsten ion is surrounded by six oxygen ions. Approximately octahedral coordination is formed. These ions can be divided into three different oxygen pairs for each cation site.

In contrast, each oxygen ion is surrounded by three cations (either two cadmium and one tungsten or two tungsten and one cadmium).

Two bands [19] were observed in the emission spectra of CdWO₄ with molybdenum impurity, [20] with the following peaks:

- at 2.46 eV (505 nm),
- peak at 1.82 eV (682 nm) corresponds to the Mo impurity at concentration 0.04%, and peak at 2.07 eV (600 nm) corresponds to the Mo at concentration 0.1%.

The 2.46 eV band is associated to trapped exciton localization (self-trapped excitons) on the WO₆ complex anions.

The 1.83 – 2.07 eV emission band is attributed to the Mo impurity defects in the crystal lattice. Mo defect reduces the light outcome of the CdWO₄ crystal what is associated with the scattering of charges on defect centres [20].

EPR spectra of molybdenum-related structure defect of CdWO₄ crystal at 20 K temperature were observed. EPR spectra of molybdenum-related structural defect were measured by using an X – band (9 GHz) EPR spectrometer equipped by a helium gas flow cryostat [5]. Studied crystal was grown by Czochralski method, contained Mo impurity concentration 5·10⁻⁵ mol.%. [4], but Mo was not added especially.

4.1.2. Results

The EPR spectrum obtained with the magnetic field oriented in the [010] direction of the CdWO_4 crystal, at 20 K and microwave frequency of 9.08 GHz is shown in Figure 4.1. (a) [5]. Angular dependencies of the spectra showed that the hyperfine splitting is almost isotropic. Only small g – factor anisotropy was observed.

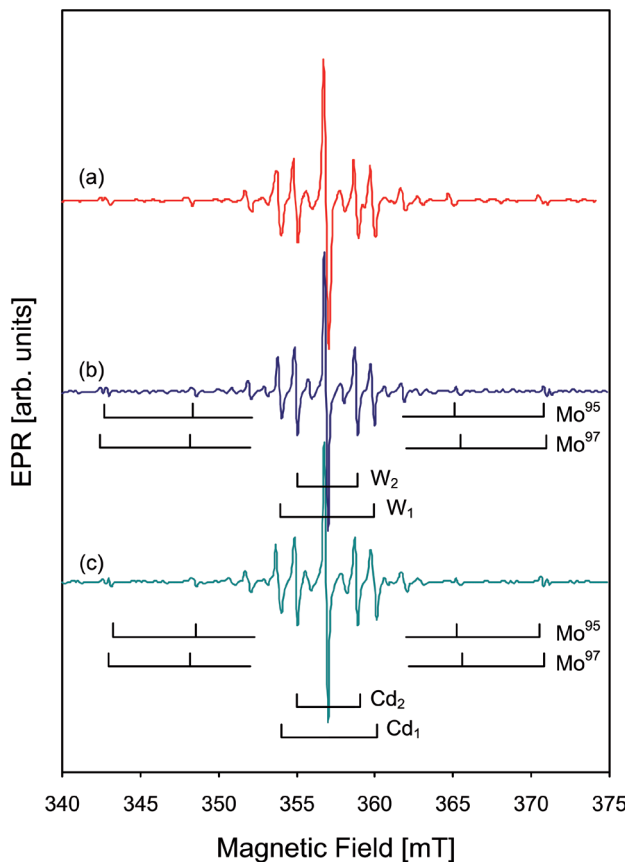


Fig. 4.1. (a) EPR spectrum of a CdWO_4 crystal, measured at 20 K for $B \parallel [010]$ applying a microwave frequency of 9.08 GHz and (b) simulated EPR spectrum with Spin-Hamiltonian parameters taken from the previous studies [5]. (c) In our study [1*] simulated EPR spectrum with Spin-Hamiltonian parameters listed in Table 4.1.

The EPR spectrum can be described by the conventional Spin-Hamiltonian:

$$\hat{H} = \mu_B \cdot \vec{S} \cdot \tilde{g} \cdot \vec{B} + \sum_{i=1}^n \vec{S} \cdot \tilde{A} \cdot \vec{I}_i$$

Hereby, the first term relates to the electron Zeeman interaction whereas the second term describes the hf interactions of the electron spin with several sets of equivalent neighbour nuclei. The EPR signals labelled Mo⁹⁵ and Mo⁹⁷, are interpreted as hf interactions of a spin $S = 1/2$ with the two molybdenum isotopes – Mo⁹⁵ ($I = 5/2$) of natural abundance of 15.9% and Mo⁹⁷ ($I = 5/2$) of natural abundance of 9.6%, respectively, and have been unambiguously identified in our previous study [5]. From two alternative interpretations of the hf lines, an interaction with two groups of equivalent W nuclei (Figure 4.1, curve b) was preferred previously [5]. However, the question arose, which of the hf lines could be attributed to interactions with Cd nuclei, because the hf interactions with Cd nuclei are usually several times stronger than hf interactions with W nuclei [21]. Therefore, presently, we return to the second alternative and analyse the EPR hyperfine structure of the Mo-related defect with account for hf interactions with two different groups of neighbouring Cd nuclei having two isotopes with nonzero nuclear spin: Cd¹¹¹ ($I = 1/2$) of natural abundance of 12.76% and Cd¹¹³ ($I = 1/2$) of natural abundance of 12.26%.

Table 4.1. Isotropic hf interaction parameters A_{iso} used for simulation of the experimental spectrum in Fig. 4.1 (c): $g[010] = 1.82$, microwave frequency 9.08 GHz, EPR line width 3 MHz.

Nucleus	Number of equivalent neighbours	Nuclear spin I	Natural abundance	A_{iso} (MHz)
Mo ⁹⁵	1	$\frac{5}{2}$	15.90%	141
Mo ⁹⁷		$\frac{5}{2}$	9.60%	144
Cd ¹¹¹	2	$\frac{1}{2}$	12.76%	97
Cd ¹¹³		$\frac{1}{2}$	12.26%	102
Cd ¹¹¹	3	$\frac{1}{2}$	12.76%	153
Cd ¹¹³		$\frac{1}{2}$	12.26%	160

The values of hf interaction constants of the isotopes are very close values and might not be resolved in our EPR spectra, in contrast to the Mo- isotope splitting which could be observed for the most distant hf lines because Mo has much higher nuclear spin value ($I = 5/2$).

4.1.3. Calculations of CdWO₄:Mo experimentally observed spectra

Spectra were simulated using the computer software program PCS. Spin-Hamiltonian describes the interaction of unpaired spin with one molybdenum nucleus and two cadmium nuclei groups (shells):

$$\hat{H} = \beta \vec{S} \tilde{g} \vec{B} + \tilde{S} \vec{A}_{Mo} \vec{I}_{Mo} + \tilde{S} \vec{A}_{Cd1} \vec{I}_{Cd1} + \tilde{S} \vec{A}_{Cd1} \vec{I}_{Cd1} + \tilde{S} \vec{A}_{Cd2} \vec{I}_{Cd2} + \tilde{S} \vec{A}_{Cd2} \vec{I}_{Cd2} + \tilde{S} \vec{A}_{Cd2} \vec{I}_{Cd2}.$$

Following input data were entered in this software:

- Spin number of unpaired electrons – $S = 1/2$,
- experimentally observed CdWO₄ g – factor has small anisotropy, therefore, in the calculation of the spectra anisotropy was not taken into account,
- g – factor is taken to be $g = 1.82$.

In these calculations we have used isotropic value of the parameters; therefore the parameters are not expressed by the tensor.

The 1st shell, which consists of one molybdenum nucleus, has 6 electron levels, the 2nd shell, which consists of two cadmium nuclei, has 4 electron levels and the 3rd shell, which consists of three cadmium nuclei, has 8 electron levels.

For the molybdenum – related defect in CdWO₄ maximum number of involved transitions is 384, if electron spin quantum number is $\Delta M_s = \pm 1$, and taking into account only “allowed” transitions with nuclei quantum number changes of $\Delta M_i = 0$.

4.1.4. Discussion

The calculation with account for 2 groups of equivalent Cd neighbours of 2 and 3 nuclei, respectively, is the best fit for the experimental spectrum. The isotropic hf parameters used in calculations are listed in Table 4.1 and the resulting spectrum is shown in Figure 4.1 (c). The coincidence with the experimental spectrum was estimated according amplitudes of the lines and distances between the lines. The present simulation (curve c) shows the same good agreement with the experimental spectrum (curve a) as the previous analysis (curve b) and we favour the present model mainly due to expected larger hf interactions with Cd nuclei in respect to W nuclei [21].

Let us consider the possible location of the unpaired spin $S = 1/2$ displaying the hf interaction with two groups of equivalent Cd nuclei. We suppose the unpaired electron has to be localised on the Mo ion. We should exclude the regular Cd, W or O sites, since the number of Cd neighbours is completely

different from the expected numbers of Cd neighbours in these sites. The most valuable solution would be interstitial molybdenum. Interstitial positions in the CdWO_4 structure [18], [22] may have 4 to 6 Cd neighbours (see Figure 4.2), which is more or less compatible with the number of 5 (2+3) Cd nuclei used in our calculations. Therefore the exact structure of the defect and its charge state still remains unclear. Further investigations with techniques like electron-nuclear double resonance (ENDOR) would be helpful to clarify remaining questions of the structure of the Molybdenum related defect in CdWO_4 .

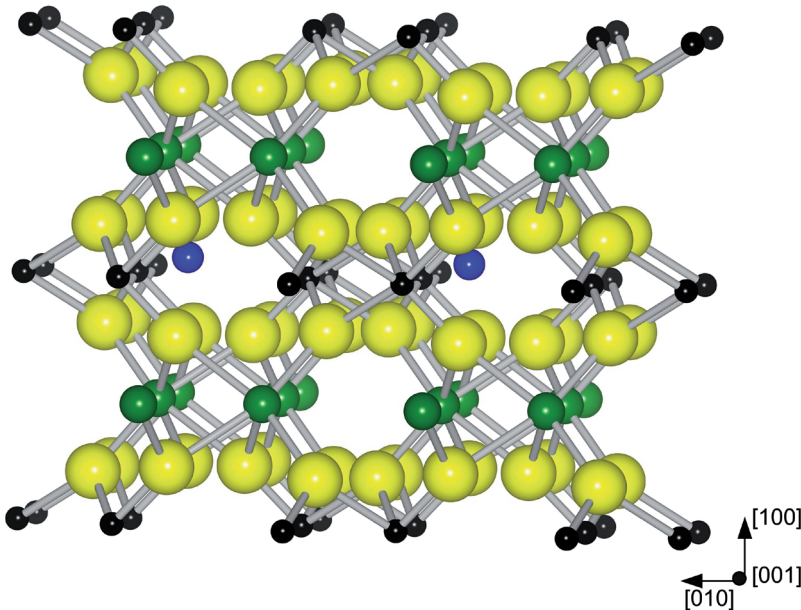


Fig. 4.2. Possible interstitial positions of molybdenum in the CdWO_4 structure.
(Mo – blue, Cd – green, W – black, O – yellow)

4.1.5. Conclusions

In the present work, we reevaluated the previous interpretation of the hf EPR spectrum of Mo-related defects in CdWO_4 . The hf structure is shown to be consistent with calculations made for an unpaired spin $S = 1/2$ interacting with two groups of 3 and 2 equivalent Cd nuclei, respectively. The unpaired spin is assumed to be localised on the Mo impurity possibly located in an interstitial position of the CdWO_4 structure [1*].

4.2. Tl-related radiation defects in CsI:Tl

4.2.1. Characteristics of CsI:Tl and Tl related defects in the crystals with NaCl structure

Caesium iodide has a base-centred, cubic structure. Caesium ion is located in the centre.

Thallium impurity ions replace caesium ions in the lattice node. At the edges the iodine ions are located.

Tl defects were investigated in detail in several alkali halide crystals with the NaCl structure. The properties of two Tl^0 – atomic defects in KCl:TlCl and NaCl:TlCl were studied using EPR and optical-absorption techniques [23]. In X-ray irradiated KCl crystals containing TlCl, ESR signals of Tl^0 , Tl^{2+} , Tl_2^+ and Tl_2^{3+} centres have been observed [24], [25]. The X-band EPR spectrum of the Tl_2^+ centre in heavily doped KCl:Tl⁺ has been identified [26]. A $\langle 111 \rangle$ – oriented Tl_2^+ centre is produced above 220 K by X-irradiation of doped KCl and RbCl [27]. The EPR of a 110 – oriented Tl_2^+ centre in NaCl and RbCl has been reported [28]. EPR detected optically via the magnetic circular dichroism of the optical absorption [12] allowed to identify and characterize the $\text{Tl}^0(1)$ and $\text{Tl}_2^0(1)$ centres in several crystals with NaCl structure [29]. Unfortunately, in EPR spectra of CsI: Tl crystals were not observed characteristic Tl centres, such as were observed in the NaCl structure.

Radiation defects in the scintillator CsI:Tl were successfully identified by EPR as V_K – centres [30], and by optically detected EPR as Tl-perturbed V_K – centres [31], [16]. The structure of no other Tl-related defect centres could be clarified. MCDA measurements revealed several Tl-related MCDA bands in X-irradiated [16] or γ -irradiated [32] CsI:Tl crystals. MCDA-EPR spectra of CsI:Tl (0.01%) X-irradiated at RT [16] detected in the 438 nm MCD band showed two groups of resonance lines, with 5–6 lines in each group, which remained unidentified due to their complicated angular dependencies.

In the present work we studied in more detail the angular dependencies of the MCD-EPR spectrum of CsI:Tl.

4.2.2. Results

Samples of CsI:Tl (0.1%) were grown in the Institute of Monocrystals, Kharkov, oriented by X-ray diffraction to allow a rotation of the magnetic field in the (110) plane and γ -irradiated at RT (up to 10^6 Gy). The magnetic circular dichroism of the optical absorption (MCDA) and the MCDA-detected electron paramagnetic resonance (MCDA-EPR) were measured in a custom-built, computer-controlled spectrometer working at 24 GHz (K-band).

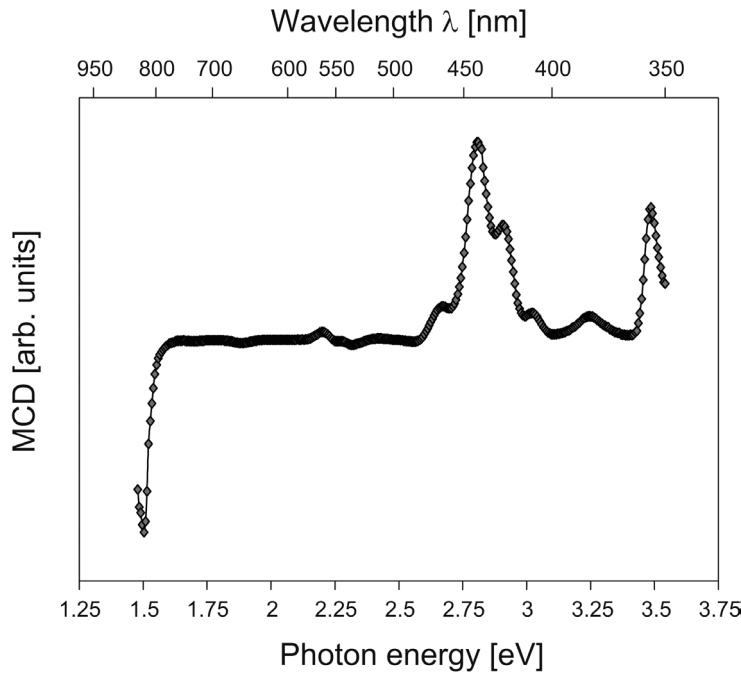


Fig. 4.3. MCDA spectrum of a CsI:Tl crystal γ -irradiated at room temperature, measured at temperature $T = 1.5$ K and $B = 2T$ [2*].

Fig. 4.3 shows the MCD spectrum of the CsI:Tl (0.1%) crystal after γ -irradiation at RT.

At least 8 MCD bands with different signs could be observed. Fig. 4.4 shows the MCDA-EPR spectrum measured in the 425 nm MCDA band. Identical MCD-EPR spectra could be measured also in the 355, 411, 442, 465, 536, and 815 nm MCDA bands [2*].

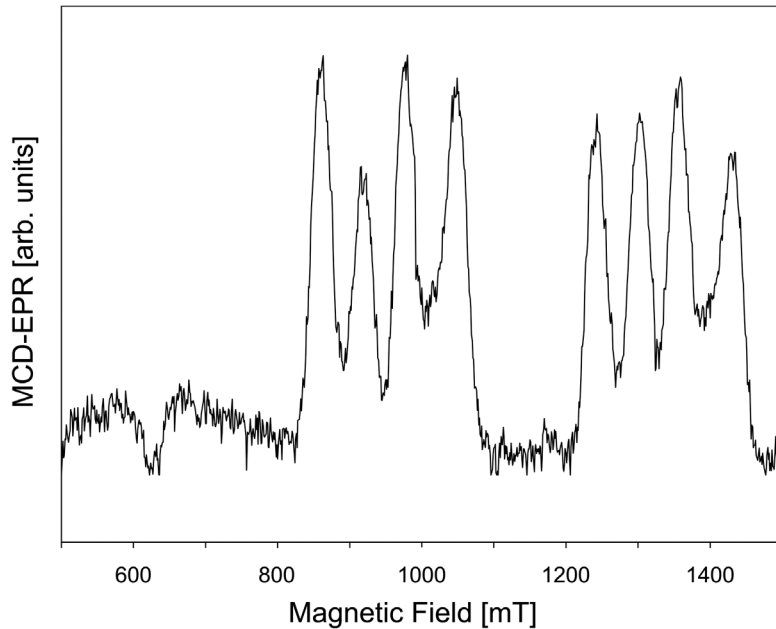


Fig. 4.4. MCD detected EPR spectrum of CsI:Tl measured in the 425 nm MCDA band. Microwave frequency was 24.32 GHz, $B \parallel [100]$, measurement temperature $T = 1.5$ K. Magnetic field dependent background is subtracted [2*].

Fig. 4.5 shows the angular dependencies of the MCD-EPR lines. The angular dependence of this spectrum simplifies at the orientation of the magnetic field $B \parallel [100]$ and consists there of 8 main nearly equally intense EPR lines (two quartets). A weaker MCD-EPR line in the lower field region at 625 mT could also be observed, with an opposite sign with respect to the main lines.

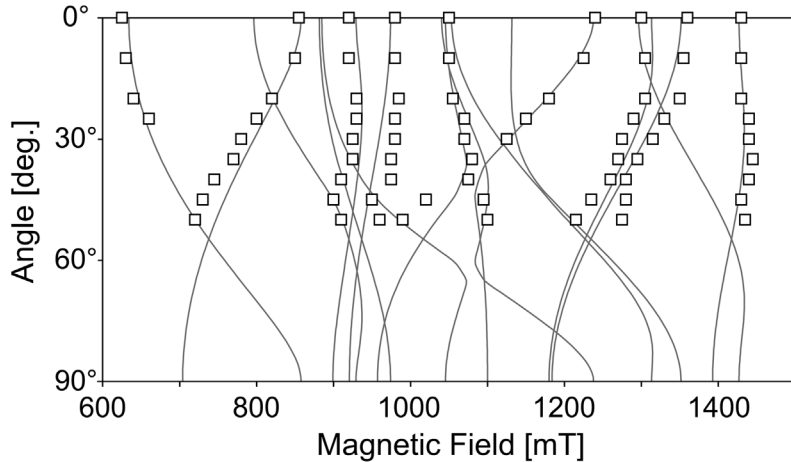


Fig. 4.5. Angular dependence of the MCDA-EPR spectra by rotation of the magnetic field in the (110) plane. Angle of 0° correspond to $B \parallel [100]$. Squares – experimental data points measured in the 425 nm MCDA band; solid lines – calculated line positions with the parameters of Table 4.2 [2*].

Experimental data points are shown in Fig. 4.5, by squares. By increasing the microwave power, additional lines between the quartets start to appear. When rotating the magnetic field away from $B \parallel [100]$ in the (100) plane, the splitting of the line quartets starts to increase and all lines overlap. For the hf interaction only nuclear spins of the Tl nuclei should be considered ($I = 1/2$, for both isotopes – ^{203}Tl and ^{205}Tl ; the nuclear g-factors are very similar and therefore the interactions of both isotopes could not been resolved in our measurements).

The actual Spin-Hamiltonian to be considered is:

$$\hat{H} = \mu_B \vec{B} \tilde{g} \vec{S} + \sum_i^3 \vec{S} \tilde{A}_i \vec{I},$$

where g and A_i are the g-tensor and hf tensors, respectively, μ_B is the Bohr magneton.

Our analysis shows that the spectra can only be explained assuming an hyperfine interaction with 3 Tl nuclei, of which two are equivalent and all hf terms are axially symmetric about a $\langle 100 \rangle$ direction (Table 4.2). In principle, for a large Tl hf interaction with one nucleus and two smaller ones with two equivalent nuclei one would expect each hf doublet line of the “larger” Tl to be split into a triplet with intensity ratio of 1:2:1.

However, due to a large anisotropic interaction and higher-order effects the “middle” line of the triplet is split and thus we observe two quartets.

Table 4.2. Spin-Hamiltonian parameters of the Tl-trimer centre, the hyperfine parameters are given in mT.

g_{\parallel}	g_{\perp}	$ A_{\parallel}^1 $	$ A_{\perp}^1 $	$ A_{\parallel}^2 $	$ A_{\perp}^2 $
1.78	1.47	144	273	214	71
± 0.02	± 0.01	± 5	± 2	± 5	± 1

Fig. 4.5 (solid curves) shows the simulated EPR spectrum with the $S = 1/2$, and an hf interaction with the three Tl nuclei (see Table 4.2). The axes of the g-tensor and all Tl-hf tensors were aligned along a $<100>$ direction.

4.2.3. Calculations of CsI:Tl spectra

Spectra were simulated using computer software program EPR-NMR.

Spin-Hamiltonian describes the interaction of unpaired spin with three thallium nuclei:

$$\hat{H} = \mu_B \vec{S} \tilde{g} \vec{B} + \vec{S} \tilde{A}_{m1} \vec{I}_{m1} + \vec{S} \tilde{A}_{m2} \vec{I}_{m2} + \vec{S} \tilde{A}_{m3} \vec{I}_{m3}.$$

Following input data were entered in this software:

Spin number of unpaired electrons: $S = 1/2$, $I_1 = 1/2$, $I_2 = 1/2$, $I_3 = 1/2$, – I2 nuclear spins numbers that describe hyperfine interaction of the unpaired electron spin and three thallium nuclei ^{203}Tl with natural abundance 29.52% and ^{205}Tl with natural abundance 70.48%.

g – tensor is a non-dimensional quantity.

In these calculations we used the axial symmetry:

$$\tilde{g} = \begin{pmatrix} g_{\perp} & 0 & 0 \\ 0 & g_{\perp} & 0 \\ 0 & 0 & g_{\parallel} \end{pmatrix},$$

A denotes the hyperfine constants. In these calculations A was given in mili Teslas.

For each Tl nucleus we have used axial symmetry of the hyperfine tensor:

$$\tilde{A}_{Tl} = \begin{pmatrix} A_{1\perp} & 0 & 0 \\ 0 & A_{1\perp} & 0 \\ 0 & 0 & A_{1\parallel} \end{pmatrix}, \quad \tilde{A}_{Tl_2} = \begin{pmatrix} A_{2\perp} & 0 & 0 \\ 0 & A_{2\perp} & 0 \\ 0 & 0 & A_{2\parallel} \end{pmatrix}, \quad \tilde{A}_{Tl_3} = \begin{pmatrix} A_{2\perp} & 0 & 0 \\ 0 & A_{2\perp} & 0 \\ 0 & 0 & A_{2\parallel} \end{pmatrix}$$

The hyperfine interaction tensor could be divided isotropic and anisotropic part:

$$A_{\parallel} = a + 2b \text{ un } A_{\perp} = a - b$$

$$a + \begin{pmatrix} -b & 0 & 0 \\ 0 & -b & 0 \\ 0 & 0 & -2b \end{pmatrix} = \begin{pmatrix} A_{\perp} & 0 & 0 \\ 0 & A_{\perp} & 0 \\ 0 & 0 & A_{\parallel} \end{pmatrix},$$

16 electron transitions has been examined, where $\Delta M = \pm 1$ is electron spin quantum number, $\Delta M_1 = 0$ is nuclear spin quantum number, taking into account only “allowed” transitions.

The calculations were performed by rotating a magnetic field (110) plane:

$$h\nu = \Delta E,$$

where ν – microwave frequency (24,32 GHz) and ΔE – energy difference between Zeeman sublevels.

4.2.4. Discussion and conclusions

The parameters shown in Table 4.2 allow us to discuss a possible defect model to explain MCDA-EPR lines. Since the g-factors are lower than $g = 2.00$, Such g-factors have been observed for atomic Tl⁰ (1) centres and the pairs Tl₂⁺, Tl₂⁰(1) centres in alkali halides with NaCl structure [29], [33], [26], [28]. Taking into account only “allowed” ($\Delta M_1 = 0$) EPR transitions we note that neither the total number of lines nor their angular dependencies can be explained by hf interactions with only two Tl – nuclei ($I = \frac{1}{2}$). However, the spectrum can be satisfactorily explained taking into account hf interactions of $S = \frac{1}{2}$ with three Tl nuclei of which two are equivalent. To explain the observed Tl hf interactions we propose the following model (see Fig. 4.6). Our spectra have some qualitative similarities with the so-called V_t – centre (electron trapped on three fluorines (F_3^{2-})) [34].

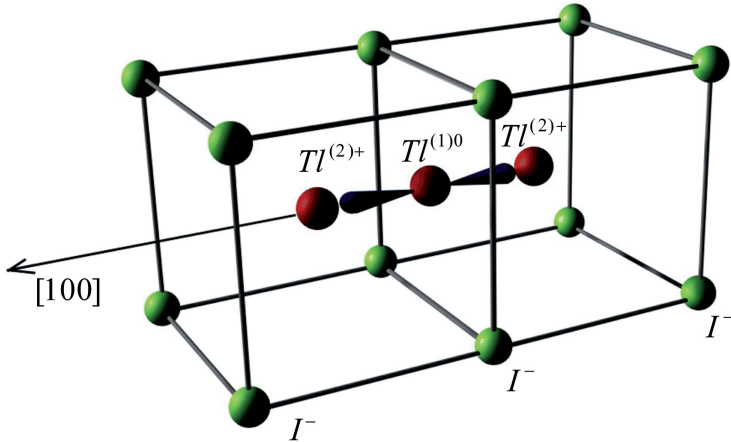


Fig. 4.6 Model of non-paired spin $S = 1$ interacting with 3 Tl nuclear spins [2*].

Table 4.3. Hf parameters a and b (in mT) with reasonable signs for the Tl-trimer centre.

	Tl ¹	Tl ²
a	-134	120
b	139	49

Two Tl⁺ replace two adjacent Cs⁺ ions and a paramagnetic Tl⁰ is located between the two Tl⁺ (Tl⁰ interstitial). The hf interactions can be explained qualitatively in a ionic model Tl⁺ – Tl⁰ – Tl⁺, whereby the unpaired electron is in a 6p orbital [100] along the direction (Tl¹ in Table 4.2). This defect is neutral with respect to the lattice. From experimental the signs of $A_{||}$, A_{\perp} cannot be determined. If the unpaired electron occupies a Tl¹ 6p orbital the anisotropic hf constant b must be positive [12]. This determine the choice of the sign of $A_{||}$ and A_{\perp} of Tl¹. In Table 4.3 the resulting isotropic and anisotropic hf constants are collected compatible with the proposed model. Since Tl 6p has a node at the Tl¹ nuclear site the isotropic hf interaction would be zero if not core polarization effects would cause an isotropic hf interaction, which is usually negative as observed [12]. The two ligands Tl² have approximately $b \approx \frac{1}{3}a$, which is typical for an overlap admixture of the Tl 6s and 6p orbitals into the Tl¹ 6p orbital. Thus, qualitatively, the ionic model Tl⁽²⁾⁺–Tl⁽¹⁾⁰–Tl⁽³⁾⁺ accounts for the observed hf interactions [2*].

4.3. Cathodoluminescence of terbium- and ytterbium- activated oxyfluoride glasses and glass ceramics

4.3.1. Characteristics of terbium- and ytterbium- activated oxyfluoride glasses and glass ceramics

Prospective applications of rare earth activated glasses and glass ceramics are in the high-energy physics, in X-ray computer tomography for industrial and medical imaging [7], and up-conversion luminescence process [8].

The advantages of glass ceramics as material for scintillators over single crystal scintillators are its low cost and large-volume/commercial production possibilities. In turn, the disadvantage is its susceptibility to radiation damage, which restricts the application of such material for precision calorimetry [35].

Glass ceramics is characterised by the properties peculiar both to fluoride crystals and glass. In oxyfluoride glass ceramics under proper thermal treatment the nano-crystallites can form [36].

The terbium-activated oxyfluoride glass is a promising material for scintillators [9]. Their efficiency improvement as compared with glass was observed after forming of glass ceramics however, no performance and decay time data have been reported.

In our present work we have studied cathodoluminescence spectra and luminescence decay times of terbium-activated oxyfluoride glasses and glass ceramics.

4.3.2. Results

Samples

We studied the cathodoluminescence spectra and decay kinetics of the oxyflouride glasses and glass ceramics samples obtained at the Institute of Solid State Physics with the following composition: $\text{SiO}_2 \cdot \text{Al}_2\text{O}_3 \cdot \text{Na}_2\text{CO}_3 \cdot \text{LaF}_3 \cdot \text{NaF}$, activated by Tb_2O_3 , TbF_3 , YbF_3 in various concentrations. The compositions of the studied scintillation glasses are shown in Table 4.4. Samples #1, #2, #3 are glass and #4, #5 – glass-ceramics materials.

Table 4.4. Composition of the samples (in mol. %). Uncertainty is approx. $\pm 1\%$.

# 1		# 2		#3, #4, #5	
40.4 %	SiO ₂	41.7 %	SiO ₂	40.6 %	SiO ₂
25.3 %	Al ₂ O ₃	26.0 %	Al ₂ O ₃	25.4 %	Al ₂ O ₃
19.2 %	Na ₂ CO ₃	19.8 %	Na ₂ CO ₃	19.3 %	Na ₂ CO ₃
9.1 %	LaF ₃	9.4 %	LaF ₃	9.1 %	LaF ₃
3.0 %	NaF	3.1 %	NaF	3.0 %	NaF
2.0 %	Tb ₂ O ₃	0.01 %	Tb ₂ O ₃	0.5 %	TbF ₃
1.0 %	YbF ₃			2.0 %	YbF ₃

Sample #4 was treated by heating at 660°C for 1 h, whereas sample #5 – by heating at 675°C for 1 h and additionally X-irradiated.

Cathodoluminescence measurements

The CL spectra and decay curves were recorded by a ΦEY-106 type photomultiplier tube and an M9003 Hamamatsu counting board with a special program.

All measurements, the IR absorption spectra and XRD measurements included, were carried out at room temperature.

Results

Figure 4.7 shows the cathodoluminescence spectra of the oxyfluoride glass and glass ceramics with various Tb³⁺ concentrations. The CL spectra have revealed the presence of the bands at: 380 nm, 415 nm, 435 nm, 460 nm, 490 nm, 545 nm, 585 nm, and 620 nm [3*].

The observed bands can be divided into ‘blue’ and ‘green’ groups, according to the blue and green regions of the spectrum. These spectral bands are attributed to the trivalent terbium luminescence. ‘Blue’ group corresponds to the terbium energy level transitions $^5D_3 \rightarrow ^7F_J$ ($J=6, 5, 4, 3$) and ‘green’ group – to the terbium energy level transitions $^5D_4 \rightarrow ^7F_J$ ($J=6, 5, 4, 3$) [37]. The band at the wavelength 490 nm could be considered as a superposition of two transitions: $^5D_3 \rightarrow ^7F_2$ and $^5D_4 \rightarrow ^7F_6$.

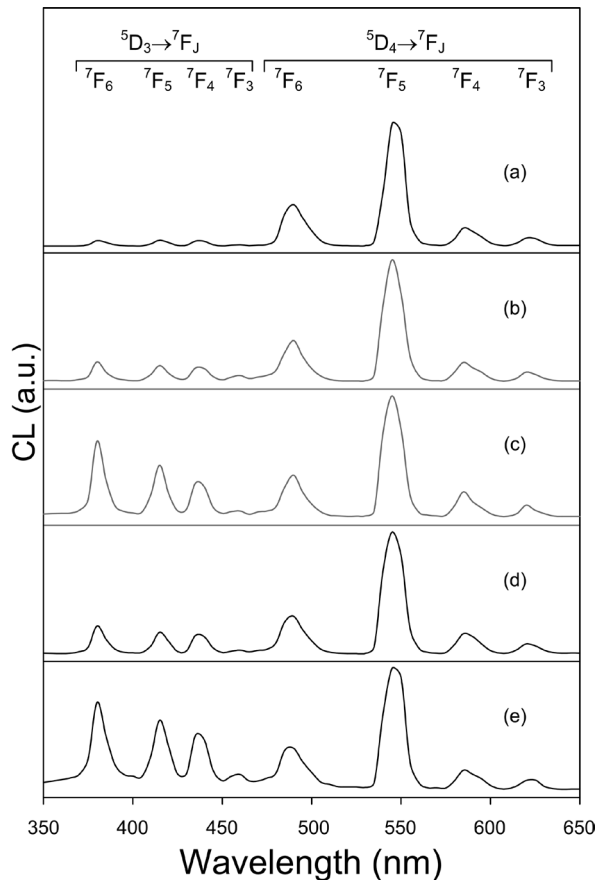


Fig. 4.7. Normalized CL spectra of the oxyfluoride samples. The curves are arranged according to the terbium concentration: #1 glass sample, Tb^{3+} 2 % (a); #5 glass ceramics sample, Tb^{3+} 0.5 % (b); #4 glass ceramic sample, Tb^{3+} 0.5 % (c); #3 glass sample, Tb^{3+} 0.5 % (d); #2 glass sample, Tb^{3+} 0.01 % (e).

We have estimated the ratio of the ‘green’ and ‘blue’ group peak intensity sums. The ratios for various terbium concentrations are listed in Table 4.5.

Table 4.5. Blue- to green-group ratio. The uncertainty is approx. ± 0.05 .

Sample	#1	#2	#3	#4	#5
Activator concentration, (%)	2Tb 1Yb	0.01 Tb	0.5Tb 2Yb	0.5Tb 2Yb	0.5Tb 2Yb
‘Blue’ and ‘green’ group ratio	0.1	1.12	0.4	0.85	0.3

The ytterbium transition from the ground state to the excited state ($^2F_{7/2} \rightarrow ^2F_{5/2}$) occurs at 978 nm [38]. No ytterbium luminescence bands were observed in the CL spectra due to measurement range limitations of the CL spectrometer. However, in the infrared absorption spectra of the samples containing Yb³⁺ ions (#1, #3, #4, #5) we observed a band at 978 nm.

The decay times of the CL measured at 380 nm, 490 nm and 545 nm have been found. The decay curves for sample #4 are shown in Fig. 4.8.

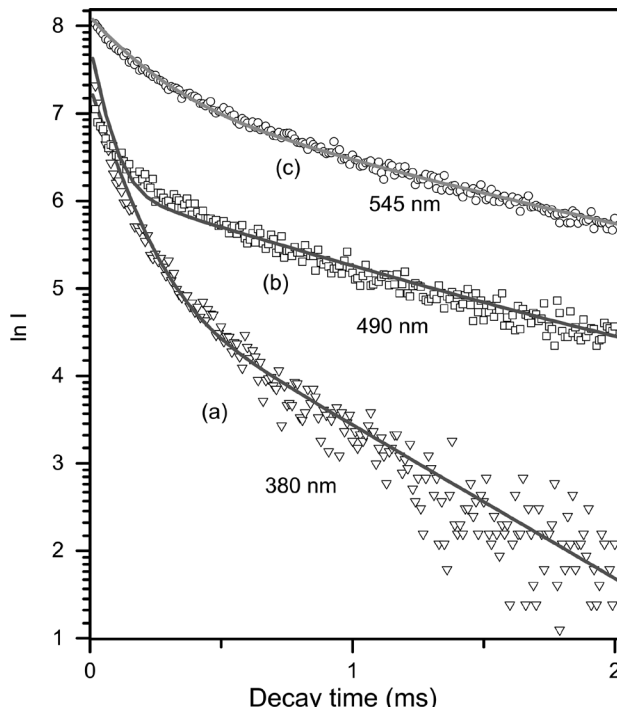


Fig. 4.8. Decay curves of sample #4 (glass ceramics): triangles – experimental points measured at 380 nm (a), squares – experimental points measured at 490 nm (b), circles – experimental points measured at 545 nm (c); solid lines – simulated curves [3*].

To fit the experimental CL decay curves for all samples two exponential functions were used:

$$f(t) = A_1 \exp(-t/\tau_1) + A_2 \exp(-t/\tau_2) + B$$

where A_i is the decay amplitude, B is a constant, τ_i is the decay time.

The decay times of the pairs of exponents are listed in Table 4.6.

Table 4.6. Exponent pairs consisting of short and long decay time components by which the experimental decay curves could be interpolated. The decay times were measured at 380 nm, 490 nm, and 545 nm. Uncertainty for the short components is $\pm 5 \mu\text{s}$, and for the long ones – $\pm 20 \mu\text{s}$.

Sample	Activator	Decay Time, μs					
		380 nm		490 nm		545 nm	
#1	2Tb, 1Yb	15	180	120	980	150	1030
#2	0.001 Tb	40	600	20	940	190	1030
#3	0.5Tb, 2Yb	30	320	100	990	150	990
#4	0.5Tb, 2Yb	100	570	55	1040	200	1210
#5	0.5Tb, 2Yb	45	570	70	1020	150	1060

For more convenient comparison of the exponential functions of different samples we have calculated the average exponents of each pair (see Table 4.7)

For this purpose the following formula was used [39]:

$$\langle \tau \rangle = \sum_{i=1}^n A_i \tau_i^2 / \sum_{i=1}^n A_i \tau_i$$

Table 4.7. The calculated average of the exponent pair. The table is arranged according to the terbium concentration. Uncertainty is approx. $\pm 15 \mu\text{s}$.

Sample	Activator	Decay Time, μs		
		380 nm	490 nm	545 nm
#1	2Tb, 1Yb	65	790	815
#3	0.5Tb, 2Yb	145	850	905
#2	0.001 Tb	330	740	975
#4	0.5Tb, 2Yb	310	860	1010
#5	0.5Tb, 2Yb	265	820	870

In our experiments the intensity of the CL spectra was not stable and decreased with time.

In the XRD measurements LaF_3 nano-size crystallites embedded in the matrix of oxide glass ceramics were observed.

4.3.3. Discussion

The Tb^{3+} in oxyfluoride glass ceramics can be embedded either in the oxide glass part or in the fluoride crystals. In the latter case (when a significant Tb^{3+} proportion is embedded in the fluoride crystals), the luminescence lifetimes should differ significantly from that of glass with the same composition, because Tb^{3+} could be located in different surroundings. However, the CL spectra of the investigated glass and glass ceramics of the same composition have nearly the same shape, with no significant difference in the decay times observed. One reason could be following - in the investigated oxyfluorides only a minor Tb^{3+} proportion is expected to be embedded in the fluoride crystal part of the ceramics.

We will discuss the luminescence intensity relations and CL decay times of the studied oxyfluoride glasses and glass ceramics samples. The ratio of the 'blue' group and 'green' group intensities decreases if the terbium concentration increases in the glass samples. This correlation could be attributed to the terbium cross-relaxation mechanism [37] between $^5\text{D}_3 \rightarrow ^5\text{D}_4$ and $^7\text{F}_6 \rightarrow ^7\text{F}_0$ transitions of two Tb^{3+} ions.

The luminescence intensity reduction with time could be attributed to the CL excitation properties as well as to the creation of colour centres affecting the luminescence.

CL decay curves can be sufficiently well approximated by two exponents: fast and slow. The experimental curves of decay time could not be fitted by the hyperbolic function or by only one exponential function. The slower decay time component can be related to the re-trapping of electrons or holes before they reach Tb^{3+} .

As the terbium concentration increases in the glass samples, the decay times of the 'blue' group decreases while those of the 'green' group do not change considerably. This could be explained by their cross-relaxation [37].

To improve the scintillation properties of Tb-doped oxyfluoride glasses and glass ceramics, further investigations are needed.

4.3.4. Conclusions

The CL spectra of the studied glasses and glass ceramics show characteristic Tb^{3+} luminescence bands ('blue' and 'green' groups). In the glass samples 'blue' to 'green' intensity ratio as well as decay times of the blue group depend on the terbium concentrations.

The CL decay curves could be sufficiently well approximated by two exponents – fast and slow.

The decay times in the blue-group CL bands are faster than in those of 'green' group, which could be explained by a cross-relaxation between Tb^{3+} ions [3*].

5. Summary

5.1. Main results

1. In this work we have clarified hyperfine interaction parameters, which explain experimental curves of the $\text{CdWO}_4:\text{Mo}$ EPR spectrum.
2. Using hyperfine interaction parameters we have constructed more precise spatial model of the Mo defect structure in $\text{CdWO}_4:\text{Mo}$ crystal.
3. In this work we have clarified hyperfine interaction parameters, which explain experimental curves of the CsI:Tl MCD-EPR spectrum.
4. Using hyperfine interaction parameters we have designed the spatial model of the Tl timer structure defect in CsI:Tl crystal.
5. By increasing Terbium concentration in the glass sample with the composition $\text{SiO}_2 - \text{Al}_2\text{O}_3 - \text{Na}_2\text{O} - \text{LaF}_3 - \text{NaF}$ in the luminescence spectra blue to green luminescence group intensity ratio and blue group decay times reduce, which could be explained by cross relaxation between transitions $^5\text{D}_3 \rightarrow ^5\text{D}_4$ and $^7\text{F}_6 \rightarrow ^7\text{F}_0$ in Tb^{3+} ions.

5.2. Thesis

1. In a model of Mo structure defect in CdWO_4 crystal unpaired spin is located in the interstitial position, on Mo impurity, where it can interact with two cadmium nuclei groups (with 3 and 2 cadmium nuclei in group).
2. CsI:Tl Tl hyperfine interactions can be explained in the following model: two Tl^+ replaces two adjacent Cs^+ ions and a paramagnetic Tl^0 is located between the two Tl^+ (Tl^0 interstitial). The unpaired electron is in a 6p orbital along the [100] direction.

5.3. Outlook

The aims and tasks of this doctoral work have been successfully completed. We have clarified the defect structure of the crystals $\text{CdWO}_4:\text{Mo}$ and CsI:Tl and luminescence properties of the terbium activated glasses and glass ceramics from viewpoint of application them as scintillators.

During this work we encountered the problem to find the most appropriate simulation program for each particular study.

For instance, due to a large number of the CdWO₄ nuclei and isotopes we could not use the most precise spectra simulation program – EPRFOR, instead we had to use the less precise program – PCS.

During studies of oxyfluoride glasses and glass ceramics, we encountered the following problems:

- Oxyfluoride radiation hardness – in repeated CL measurements were observed intensity changes.
- We could not unambiguously determine how the heating of the samples influences activated oxyfluoride properties.
- The complicated CL decay curves, what we sufficiently well approximate by two exponents, which are different for each measurement.

Our designed Tl timer defect model in CsI: Tl crystal could be considered as sufficiently completed, although CsI: Tl structure still has a number of other structural defects of Tl centers that have not been clarified yet.

CdWO₄ defect structure model could be clarified by obtaining additional information from other magnetic resonance techniques such as ENDOR.

In further investigations we plan to prepare the activated oxyfluoride compositions with improved luminescence properties which could be studied using the EPR in order to determine defect structure.

6. List of author's publications

- [1*] E. Elsts and U. Rogulis, *EPR hyperfine structure of the Mo-related defect in CdWO₄*, phys. stat. sol. (c) 2, 2005, p. 69.
- [2*] U. Rogulis, J.-M. Spaeth, E. Elsts, A. Dolgopolova, *Tl-related radiation defects in CsI:Tl*, *Radiation Measurements*, 38, 2004, p. 663.
- [3*] E. Elsts, U. Rogulis, J. Jansons, A. Sarakovskis, *Cathodoluminescence of terbium and ytterbium activated oxyfluoride glasses and glass ceramics*, Latvian Journal of Physics and Technical Sciences, 5, 2010, p. 48.
- [4*] A. Fedotovs, E. Elsts, U. Rogulis, I. Tale, M. Nikl, N. Ichinose, K. Shimamura, *EPR of F type centres in LiBaF₃*, Proceedings of the international Conference on Inorganic Scintillators and their Industrial Applications SCINT'2005, Alushta, Ukraine, 2006, p. 156.
- [5*] A. Fedotovs, E. Elsts, U. Rogulis, A. Gulans, I. Tale, M. Nikl, N. Ichinose, K. Shimamura, *EPR Hyperfine Structure of F-type Centres in Pure LiBaF₃ Crystal*, physica status solidi (c)4/3, 2007, p. 1284.

7. List of conference abstracts

International conferences

1. U. Rogulis, J.-M. Spaeth, E. Elsts, A. Dolgopolova, *Tl-related radiation defects in CsI:Tl*, 5th European Conference on Luminescent Detectors and Transformers of Ionizing Radiation LUMDETR'2003, Book of Abstracts. p.191.
2. E. Elsts and U. Rogulis, *EPR hyperfine structure of the Mo-related defect in CdWO₄*, 15th International Conference on Defects in Insulating Materials ICDIM' 2004, Riga, Book of Abstracts p. 98.
3. A. Fedotovs, E. Elsts, U. Rogulis, I. Tale, M. Nikl, N. Ichinose, K. Shimamura, *EPR of F type centres in LiBaF₃*, Conference on Inorganic Scintillators and their Industrial Applications SCINT'2005, Alushta, Book of Abstracts, p. 60.
4. A. Fedotovs, E. Elsts, U. Rogulis, A. Gulans, I. Tale, M. Nikl, N. Ichinose, K. Shimamura, *EPR hyperfine structure of F-type centres in pure LiBaF₃ crystal*, 10th Europhysical Conference on Defects in Insulating Materials EURODIM' 2006, Milano, Book of Abstracts, p. 340.

Local conferences

5. E. Elsts, U. Rogulis, *EPR spektru hipersīkstruktūra CsI:Tl*. LU CFI 19. Zinātniskās Konferences tēzes, 2003, 64. lpp.
6. E. Elsts, U. Rogulis, *Par Mo defekta EPR hipersīkstruktūru CdWO₄*, LU CFI 20. Zinātniskās Konferences tēzes, 2004, 87. lpp.
7. E. Elsts, U. Rogulis, A. Fedotovs, *SrF₂:Ce Kristālu EPR spektri*, LU CFI 21. Zinātniskās Konferences tēzes, 2005, 8. lpp.
8. E. Elsts, A. Fedotovs, U. Rogulis, A. Guļāns, I. Tāle, M. Nikl, N. Ichinose, K. Shimamura, *F - tipa centru EPR tīrā LiBaF₃ kristālā*, LU CFI 22. Zinātniskās Konferences tēzes, 2006, 8. lpp.
9. E. Elsts, U. Rogulis, *Defektu centru magnētisko rezonanšu pētījumi luminiscento detektoru materiālos*, LU CFI 25. Zinātniskās Konferences tēzes, 2009, 92. lpp.
10. E. Elsts, U. Rogulis, J. Jansons, A. Šarakovskis, *Ar terbiju un iterbiju aktivētu oksifluorīdu stiklukeramiku katodluminiscence*, LU CFI 26. Zinātniskās Konferences tēzes, 2010, 11. lpp.

8. References

- [1] L. Nagornaya, G. Onyshchenko, E. Pirogov, N. Starzhinskiy, I. Tupitsyna, V. Ryzhikov, Yu. Galich, Yu. Vostretsov, S. Galkin and E. Voronkin, *Production of the high-quality CdWO₄ single crystals for application in CT and radiometric monitoring*, Nuclear Instruments and Methods in Physics Research A, Vol. 537, 2005 , p. 163.
- [2] M.-J. van Goethem, M.S. Wallace, B.E. Nett, M.A. Famiano, K.R. Herner, D.J. Oostdyk, M. Mocko, W.G. Lynch, M.B. Tsang, P. Schotanus, J. Telfer, H.L. Clark, A. Moroni, R. de Souza and L.G. Sobotka, *Investigations and corrections of the light output uniformity of CsI(Tl) crystals*, Nuclear Instruments and Methods in Physics Research A, 526, 2004, p. 455.
- [3] B.-J. Kim, B.K. Cha, H. Jeon, Y.K. Chi and G. Cho, *A study on spatial resolution of pixelated CsI(Tl) scintillator*, Radiation Measurements, 42, 2007, p. 1415.
- [4] A.E. Ovechkin, L.L. Nagornaya, I.A. Tupitsina, and Ya.Ya. Vostretsov, *Colour centres in CdWO₄ crystals*. Journal Prikladnoi Spektroskopii (in Russian) 51, 1989, p. 146.
- [5] U. Rogulis, *EPR of molybdenum-related defect in CdWO₄ crystal*, Radiation Measurements, 29, 1998, p. 287.
- [6] V. Nagirnyi, A. Stolovich, S. Zazubovich, V. Zepelin, E. Mihokova, E. Nikl, G.-P. Pazzi, L. Salvini, *Peculiarities of the triplet relaxed excited-state structure and luminescence of a CsI:Tl crystal*. J. Phys.: Condens. Matter 7, 1995, p. 3637.
- [7] J. Fu, M. Kobayashi and J.M. Parker, *Terbium-activated heavy scintillating glasses*, J. Lumin., 128, 2008, p. 99.
- [8] M.J. Dejneka, *Transparent oxyfluoride glass ceramics*, MRS Bull. 23, 1998, p. 57.
- [9] Z. Pan, K. James, Y. Cui, A. Burger, N. Cherepy, S.A. Payne, R. Mu, S.H. Morgan, *Terbium-activated lithium-lanthanum-aluminosilicate oxyfluoride scintillating glass and glass-ceramic*, Nucl. Instr. and Meth. in Phys. Res. A 594, 2008, p. 215.
- [10] Р. Бикбуталов, *Казанские истории*, 7–8, 2004, <http://www.1000kzn.ru/article/ru/2915/383/1/>
- [11] А.С. Марфунин, *Спектроскопия, люминесценция и радиационные центры в минералах*, Недра, 1975, с. 327.
- [12] J.-M. Spaeth, H. Overhof, *Point defects in Semiconductors and Insulators*, Springer, 2003, 490 p.

-
- [13] W.R. Hagen, *Biomolecular EPR Spectroscopy*, CRC Press, 2008 248 p.
 - [14] U. Rogulis, A. Fedotovs, *Elektronu paramagnētiskā rezonanse (EPR). Laboratorijas darba apraksts LU maģistrantūras studentiem*, 2005, Rīga
 - [15] V. Ogorodiņiks, *Radiācijas defektu pētījumi ar EPR metodi LiBaF_3* , Promocijas darbs, 2004, Riga
 - [16] W. Meise, *Lumineszenz und Strahlenschädigungen von CsJ:Tl^+ Röntgenszintillatoren*, Diploma Thesis, 1988, Paderborn.
 - [17] M.J. Mombourquette, J. A. Weil, *Operating instructions for computer program EPR-NMR*, University of Saskatchewan, Canada, 2004.
<http://homepage.usask.ca/~jaw519/>
 - [18] R.W.G. Wyckoff, *Crystal Structures*, 2nd edn., Interscience, 3, 1965, p. 42.
 - [19] Kotlov, L. Jönsson, H. Kraus, V. Mikhailik, V. Nagirnyi, G. Svensson and B.I. Zadneprovski, *Excited states of molybdenum oxyanion in scheelite and wolframite structures*, Radiation Measurements, 42, 2007, p. 767.
 - [20] S.N. Ivanov, V.N. Kolobanov, V.V. Mikhailin, O.V. Rzhevskaya, D.A. Spassky, B.I. Zadneprovski, L. Jonsson, G. Svensson, *Luminescence of the set of tungstate crystals with wolframite structural type*, Proceedings of the 8th International Conference on Inorganic Scintillators and their Use in Scientific and Industrial Applications. Kharkov, 2006, p. 375
 - [21] J.R. Morton, and K.F. Preston, *Atomic parameters for paramagnetic resonance data*, Journal of Magnetic Resonance, 30, 1978, p. 577.
 - [22] Watterich, G.J. Edwards, O.R. Gilliam, L.A. Kappers, D.P. Madacs, K. Raksanyi, and R. Voszka, *ESR of platinum impurity ions in ZnWO_4 single crystals* Journal of Physical Chemistry of Solids, 52, 1991, p. 449.
 - [23] Heynderickx, E. Goovaerts, S.V. Nistor and D. Schoemaker, *Site-switched Tl^0 atoms in Tl^{+} -doped NaCl and KCl* , Phys. Rev. B, 33, 1985, p. 1559.
 - [24] Y. Toyotomi and R. Onaka, *Trapped Electron Centre and Trapped Hole Centres in Heavily Doped KCl:Tl : I. Thermal Glow Study*, Journal of the Physical Society of Japan, 46, 1978a, p. 1861.
 - [25] Y. Toyotomi and R. Onaka, *Trapped Electron Centre and Trapped Hole Centres in Heavily Doped KCl:Tl : II. ESR Study*, Journal of the Physical Society of Japan, 46, 1978b, p. 1869.
 - [26] B.-r. Yang, E. Goovaerts, and D. Schoemaker, *Identification and analysis of the Tl^{2+} ESR spectrum in KCl:Tl^+* , Phys. Rev. B, 27, 1983, p. 1507.

-
- [27] S.V. Nistor, E. Goovaerts, B.-r. Yang and D. Schoemaker, *Interstitial Tl⁰ atoms in alkali halides: ESR study of a <111>- oriented Tl²⁺ centre*, Phys. Rev. B, 28, 1983, p. 1219.
 - [28] S.V. Nistor, D. Schoemaker, I. Ursu and B.-r. Yang, *The study of Tl²⁺<110> centres in NaCl and RbCl*, phys. stat. sol. (b), 127, 1985, p. 503.
 - [29] F.-J. Ahlers, F. Lohse, and J.-M. Spaeth, *Identification of a Tl dimer centre in alkali halides by ODMR*, J. of Physics C, 18, 1985, p. 3881.
 - [30] J.J. Pilloud, and C. Jaccard, *ESR of V_K centers in CsI*, Solid State Commun. 17, 1975, p. 907.
 - [31] J.-M. Spaeth, W. Meise, and K.S. Song, *The nature of x-ray-induced luminescence and the hole centres in CsI:Tl studied by optically detected electron paramagnetic resonance*, J. Phys.: Condens. Matter, vol. 6, 1994, p. 3999.
 - [32] A.V. Dolgopolova, P.A. Kulis, V.V. Masalskis, U.T. Rogulis, N.N. Smirnov and V.G. Tale, *Spectroscopy of activator traps in CsI:Tl*, Proceedings of the international symposium Lumdetr'91, Riga, 1991, C47.
 - [33] F.-J. Ahlers, and J.-M Spaeth, *Ground and excited states of laser-active Tl⁰⁽¹⁾ centres in alkali halides*, J. of Physics C, 19, 1986, p. 4693.
 - [34] M.N. Cohen, W. Känzig, and T. O. Woodruff, *The hyperfine structure of the V_t- center*, J. Phys. Chem. Solids, 11, 1959, p. 120.
 - [35] M.J. Weber, *Inorganic scintillators: today and tomorrow*, J. Lumin. 100, 2002, p. 35.
 - [36] Z.J. Hu, Y.S. Wang, F. Bao and W.Q. Luo, *Crystallization behavior and microstructure investigations on LaF₃ containing oxyfluoride glass ceramics*, J. Non-Cryst. Solids 351, 2005, p. 722.
 - [37] H. Guo, *Photoluminescent properties of CeF₃:Tb³⁺ nanodiskettes prepared by hydrothermal microemulsion*, Appl. Phys. B84, 2006, p. 365.
 - [38] Lupei, V. Lupei, C. Presura, V. N. Enaki and A. Petraru, *Electron-phonon coupling effects on Yb³⁺ spectra in several laser crystals*, J. Phys.: Condens. Matter 11, 1999, p. 3769.
 - [39] C. Tiseanu, V.A. Lórenz-Fonfría, A. Gessner, M.U. Kumke and B. Gagea, *Comparative luminescence study of terbium-exchanged zeolites silylated with alkoxy silanes*, J. Mater. Sci.: Mater. Electron. 20, 2007, p. 312.

Acknowledgements

The author is grateful to his scientific supervisor, co-authors, colleagues, his family, his superiors, which allowed me working at ISSP, and those who influenced me to focusing on scientific researches.